JVST B
Journal of Vacuum Science & Technology B

Investigation of a defect in the β-Ga_2O_3 substrate material from capacitance transients

Cite as: J. Vac. Sci. Technol. B **40**, 064001 (2022); https://doi.org/10.1116/6.0002045
Submitted: 28 June 2022 • Accepted: 19 September 2022 • Published Online: 25 October 2022

Jian V. Li, Adam T. Neal, Shin Mou, et al.

JVST B
Journal of Vacuum Science & Technology B
ARTICLE
avs.scitation.org/journal/jvb

Investigation of a defect in the β-Ga_2O_3 substrate material from capacitance transients

Cite as: J. Vac. Sci. Technol. B **40**, 064001 (2022); doi: 10.1116/6.0002045
Submitted: 28 June 2022 · Accepted: 19 September 2022 ·
Published Online: 25 October 2022

Jian V. Li,[1,2,a),b)] Adam T. Neal,[1] Shin Mou,[1] and Man Hoi Wong[3]

AFFILIATIONS

[1] Air Force Research Laboratory, Materials and Manufacturing Directorate, Wright-Patterson AFB, Ohio 45433
[2] Azimuth Corporation, Beavercreek, Ohio 45324
[3] Department of Electrical and Computer Engineering, University of Massachusetts Lowell, Lowell, Massachusetts 01854

[a)] **Author to whom correspondence should be addressed:** jian.li.1.ctr@us.af.mil
[b)] Previously at National Cheng Kung University, Tainan, Taiwan.

ABSTRACT

The defect ~0.8 eV below the conduction band edge of β-Ga_2O_3 wide bandgap semiconductor is investigated using the matched Arrhenius-equation projection technique that offers substantial improvement over the conventional deep level transient spectroscopy technique. An experimental technique is developed to extract activation energy E_a and attempt-to-escape frequency ν_0 of defects bypassing both the rate-window treatment and the Arrhenius plot. Only raw capacitance transients in the time domain are needed with this technique. The capacitance transients are projected between the temperature and time domains as well as to E_a and ν_0 domains. Extraction of E_a and ν_0 is accomplished by matching the projected and experimental capacitance transients to each other.

Published by AIP Publishing. https://doi.org/10.1116/6.0002045

I. INTRODUCTION

β-Ga_2O_3 is a wide bandgap semiconductor material[1–4] that is projected to greatly impact next-generation power electronics,[5–7] radio-frequency electronics,[8–10] and sensing[11] devices. Electronic defects in this material[12] are among the most pressing issues that limit the performance of state-of-the-art devices at present and in the foreseeable future. Electronic defects[13,14] have been observed at 0.6, 0.8, and 1.1 eV below the conduction band edge. These defects are considered to affect the doping compensation,[15] leakage current, and threshold stability in Ga_2O_3 transistors.[16] Recent evidence[17] indicates Fe and Mg as possible causes for the defects 0.8 and 1.0 eV below the conduction band edge, respectively. Obviously, improvement of the measurement accuracy and expediency for the activation energy E_a and the capture cross section of defects is vital to understand their physiochemical origins and devising mitigation strategies in β-Ga_2O_3 material and device engineering.

Detection of β-Ga_2O_3 defects (in various forms such as Hall,[18] conductivity,[18] admittance spectroscopy,[18,19] deep-level transient spectroscopy, and DLTS,[20] sometimes assisted by optical excitation)[14] is commonly accomplished by inspecting the electrical charge response, which is based on the Arrhenius behavior of rate ν (i.e., the reciprocal of the characteristic time τ) of the carrier emission process from a defect,[18–20]

$$\nu = 1/\tau = \nu_0 \exp(-E_a/k_B T), \tag{1}$$

where ν_0 is the attempt-to-escape frequency (directly related to the carrier capture cross section),[18] k_B is the Boltzmann constant, and T is the temperature. All thermally activated electrical charge response measurements are analyzed by the conventional Arrhenius plot line-fitting procedure, where one constructs an Arrhenius plot of ln(ν) versus T^{-1} (following the common practice of neglecting the T^2 term in ν tolerating a small error $\sim k_B T$ in E_a, see Eq. (7.19) of Ref. 18 and extract E_a from the slope and ν_0 the intercept of a line fitting according to Eq. (1)]. Fitting the Arrhenius plot by a line is based on the assumption that E_a and ν_0 are invariant over the scanned range of temperature, which may be at times untrue,[21] especially for defects in wide bandgap semiconductors,[22–24] such as Ga_2O_3.

In this work, we demonstrate the measurement of E_a and ν_0 of the defect located 0.8 eV below the conduction band edge in the Ga_2O_3 substrate material using the matched Arrhenius-equation projection method. The defect is detected and analyzed not from the rate-window-treated DLTS spectra but directly from raw capacitance transients, which can be readily acquired by general-purpose instruments such as impedance analyzers and lock-in amplifiers. We extract E_a and v_0 by matching the isothermal capacitance transients to a virtual transient projected to other parameter domains, thus bypassing the rate-window treatment, the peak identification in DLTS spectra, and the Arrhenius plot construction and line fitting. The efficient utilization of information from the 2D temperature-time domain allows operation in a smaller temperature range and extraction of the temperature dependence of E_a and v_0.

II. EXPERIMENT

The β-Ga_2O_3 Schottky devices were fabricated on $(\overline{2}01)$ bulk substrates grown by edge-defined film-fed growth[25] commercially available from Tamura in Japan. After dicing the 2-in. wafer into $1 \times 1\,\text{cm}^2$ pieces, samples were cleaned in solvents (acetone, toluene, acetone, isopropyl alcohol, and then nitrogen blow dry; 5 min for each step) and 50 nm/1000 nm Ti/Au contacts were sputtered as ohmic contacts. The samples were then annealed in a tube furnace with the argon gas flow to reduce the contact resistance, the temperature being ramped up from room temperature to 450 °C in 15 min. Schottky diodes of various sizes ranging from 0.1 to $2\,\text{mm}^2$ were prepared by depositing 150 nm Au contact without additional annealing. More details of the sample preparation can be found in Ref. 26. Room-temperature capacitance-voltage measurement conducted at 10 kHz determines a carrier concentration of $n = (1.27 \pm 0.02) \times 10^{17}\,\text{cm}^{-3}$.

We used a Keithley 4200A-SCS parameter analyzer, which is an instrument commonly seen in semiconductor laboratories, to measure capacitance transients. The core piece of this system pertaining to this work is a multifrequency capacitance unit capable of acquiring data at a time resolution of ∼30 ms and over a recording time of 72 h limited by the buffer size of the data acquisition system. The frequency and AC modulation amplitude of capacitance measurements were fixed at 10 kHz and $50\,\text{mV}_{\text{peak-to-peak}}$, respectively. For temperature-dependent measurements, we mounted the sample onto a hot plate in atmospheric ambient to vary the temperature from 290 to 330 K in 5 K steps. The combination of a Keithley 4200A-SCS parameter analyzer and a hot plate with near-room temperature operability is a notable deviation and cost reduction from a commercial DLTS apparatus integrated with a cryogenic system.

After reaching a stable sample temperature, the DC bias voltage on the Ga_2O_3 Schottky junction device was fixed at +0.5 V forward bias for a period longer than 10 min to allow equilibration of charge occupancy in interested defects. The Keithley 4200A-SCS parameter analyzer was configured to collect capacitance transients from 0.2 to ∼200 s after the DC bias voltage was switched from +0.5 V forward bias to −10 V reverse bias. Figure 1 shows capacitance transients that exhibit single-exponential transient $\Delta C(t) = \Delta C_0 \exp(-t/\tau)$ toward a baseline, where ΔC_0 is the transient magnitude and τ is the carrier emission characteristic time described in Eq. (1) and extractable via curve fitting.[27] The Arrhenius plot of the characteristic time τ [i.e., $\ln(\tau)$ versus the inverse temperature, Fig. 4 in Ref. 27] can be line-fitted to extract the defect activation energy $E_a = 810 \pm 5$ meV from the slope and the attempt-to-escape frequency $\ln(v_0) = 27.7 \pm 0.2\,\text{s}^{-1}$ from the intercept with the ordinate.

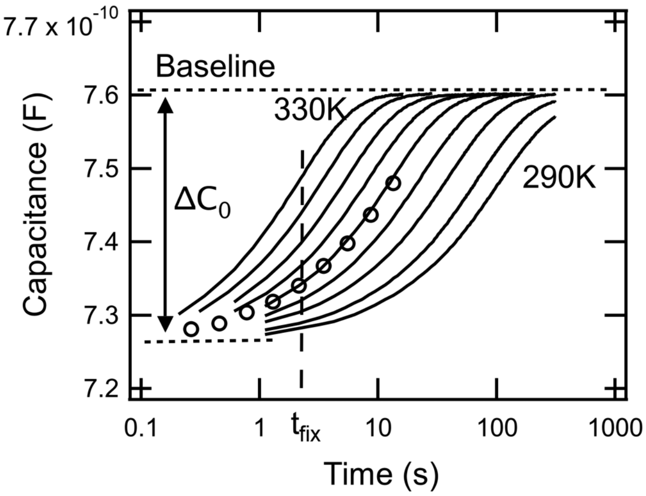

FIG. 1. Experimental isothermal capacitance transients (time axis in the logarithmic scale) measured at fixed temperatures from 290 to 330 K in 5 K steps exhibit exponential transients with a magnitude of ΔC_0. Electronics-induced baseline shift was corrected by aligning the long-time baselines. The capacitance data at $t_{fix} = 2.1$ s, indicated by the vertical dashed line, are used to reconstruct an isotime transient from which a virtual isothermal transient (symbols) are obtained [via T-t projection in Eq. (4) with $E_a' = 810$ meV] to match the isothermal transient at $T_{fix} = 310$ K.

III. RESULTS AND DISCUSSION

We define the isothermal capacitance transient taken at a fixed temperature T_{fix},

$$\begin{aligned}\Delta C(t, T_{fix}) &= \Delta C_0 \exp(-t/\tau) \\ &= \Delta C_0 \exp[-t v_0 \exp(-E_a/k_B T_{fix})],\end{aligned} \tag{2}$$

and the isotime capacitance transient taken at a fixed time t_{fix},

$$\Delta C(t_{fix}, T) = \Delta C_0 \exp[-t_{fix} v_0 \exp(-E_a/k_B T)]. \tag{3}$$

Isothermal capacitance transients measured at various temperatures are shown in Fig. 1 from which an isotime capacitance transient may be reconstructed (for example, with capacitance data taken at a fixed measurement time $t_{fix} = 2.1$ s). We extend the temperature-time duality[28,29] to capacitance transients in the form of T-t projection derived from equating Eqs. (2) and (3),

$$t_T = t_{fix} \exp[E_a' k_B^{-1}(T_{fix}^{-1} - T^{-1})], \tag{4}$$

where E_a' is used instead of E_a to indicate a free-tuning parameter. For an isotime transient $\Delta C(t_{fix}, T)$, one can apply T-t projection to project it from T-domain to t-domain and obtain a corresponding virtual isothermal transient $\Delta C(t_T, T_{fix})$ "measured" at $T = T_{fix}$,

$$\Delta C(t_T, T_{fix}) = \Delta C_0 \exp[-t_T n_0 \exp(-E_a'/k_B T_{fix}) \exp((E_a' - E_a)/k_B T)]. \tag{5}$$

The condition for the virtual transient $\Delta C(t_T, T_{fix})$ in Eq. (5) to match the experimental isothermal transient $\Delta C(t, T_{fix})$ in Eq. (2) is $E_a' = E_a$. The T-t projection is applied (using $E_a' = 810$ meV and $T_{fix} = 310$ K) to isotime $\Delta C(t_{fix}, T)$ data taken at $t_{fix} = 2.1$ s to obtain the virtual isothermal transient $\Delta C(t_T, T_{fix})$ (symbols in Fig. 1), which is in good agreement with the experimental isothermal transient $\Delta C(t, T_{fix} = 310$ K$)$.

We then reverse T-t projection by dividing a rearranged form of Eq. (1) [Ref. 29, Eq. (3)] for an isothermal process with a variable time t, i.e., $T_t = E_a/k_B/[\ln(\nu_0) + \ln(t)]$, by that at the fixed point (T_{fix}, t_{fix}), i.e., $T_{fix} = E_a/k_B/[\ln(\nu_0) + \ln(t_{fix})]$, to arrive at t-T projection,

$$T_t = T_{fix}[(\ln(\nu_0') + \ln(t_{fix}))]/(\ln(\nu_0') + \ln(t)], \tag{6}$$

where ν_0' is used instead of ν_0 to indicate a free-tuning parameter. For an experimental isothermal transient $\Delta C(t, T_{fix})$, one can apply t-T projection to project it from t-domain to T-domain and obtain a corresponding virtual isotime transient $\Delta C(t_{fix}, T_t)$ "measured" at $t = t_{fix}$. Figure 2 illustrates the application of t-T projection $[\ln(\nu_0') = 27.7\ \mathrm{s}^{-1}$ and $t_{fix} = 2.1$ s$]$ to the experimental isothermal transient $\Delta C(t, T_{fix} = 310$ K$)$ to obtain the virtual isotime transient $\Delta C(t_{fix}, T_t)$ that matches the experimental isotime transient $\Delta C(t_{fix} = 2.1$ s$, T_t)$ when $\nu_0' = \nu_0$ [the proof is omitted since it is similar to that for T-t projection described in Eqs. (2)–(5)]. After either E_a or ν_0 is determined from the above procedure via either T-t or t-T projection and matching, one can calculate the other parameter from Eq. (1) with τ extracted from experiment (e.g., by exponential fitting of the isothermal transient at $T = T_{fix}$). The above two procedures extract E_a and ν_0 by projecting one experimental capacitance transient (e.g., isothermal transient in t-domain) to the orthogonal variable domain (e.g., T-domain) and matching the resultant virtual capacitance transient to another experimental transient in this domain.

Next, we project isotime capacitance transients to a virtual activation energy domain via T-E_a projection derived from rearranging Eq. (1) for an isotime process with a variable temperature T,

$$E_{a,T} = k_B T[\ln(\nu_0'') + \ln(t_{fix})], \tag{7}$$

and the isothermal capacitance transients to a virtual activation energy domain via t-E_a projection derived from rearranging Eq. (1) for an isothermal process with a variable time t,

$$E_{a,t} = k_B T_{fix}[\ln(\nu_0'') + \ln(t)], \tag{8}$$

where ν_0'' is a free-tuning parameter. Figure 3 shows the virtual transient $\Delta C(E_{a,t})$ in the E_a domain produced by projecting the experimental isothermal transient $\Delta C(t, T_{fix})$ taken at $T_{fix} = 310$ K using t-E_a projection in Eq. (8). Figure 3 also shows the virtual transient $\Delta C(E_{a,T})$ in the E_a domain obtained by projecting the isotime transient $\Delta C(T, t_{fix})$ taken at $t_{fix} = 2.1$ s (Fig. 2) using T-E_a projection in Eq. (7). A good agreement is reached between $\Delta C(E_{a,t})$ and $\Delta C(E_{a,T})$ when the best fit attempt-to-escape frequency value of $\ln(\nu_0'') = 27.7\ \mathrm{s}^{-1}$ is used in both Eqs. (7) and (8), in agreement with that extracted from the

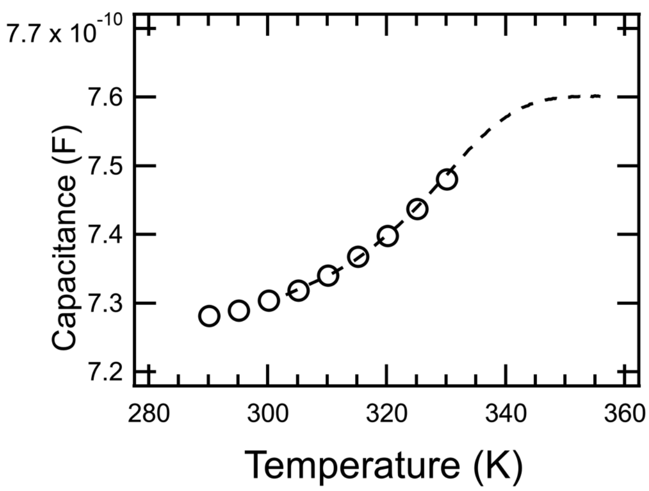

FIG. 2. Isotime capacitance transient at $t_{fix} = 2.1$ s (symbols) is constructed from the intercepting points between the vertical line and the isothermal transients in Fig. 1. The virtual isotime transient (dashed line) $\Delta C(t_{fix}, T_t)$ projected from the isothermal transient measured at $T_{fix} = 310$ K using the t-T projection [Eq. (6)] with the best fit value $\ln(\nu_0') = 27.7\ \mathrm{s}^{-1}$.

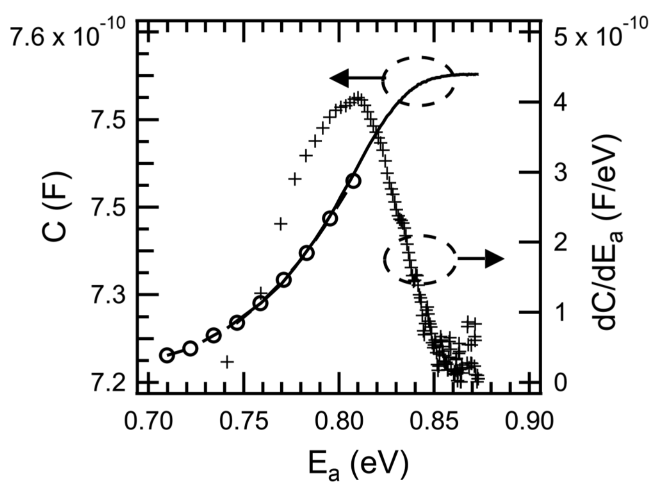

FIG. 3. Isothermal and isotime transient taken at $T_{fix} = 310$ K and $t_{fix} = 2.1$ s, respectively, are projected onto the E_a domain by Eqs. (8) and (7) using the best fit value of $\ln(\nu_0'') = 27.7\ \mathrm{s}^{-1}$ to produce good matching between the virtual transients of $\Delta C(E_{a,t})$ (solid line) and $C(E_{a,T})$ (dashed line and circles). E_a is extracted directly from the peak position of $d\Delta C(E_{a,t})/dE_{a,t}$ (crosses).

conventional Arrhenius plot. Next, E_a can be extracted directly (a straightforward proof based on elementary calculus is omitted here) from the peak position of $dC(E_{a,T})/dE_{a,T}$ or $dC(E_{a,t})/dE_{a,t}$, and the latter is shown in Fig. 3 as an example.

The electrical instrument (Keithley 4200A-SCS) and experimental configuration of this work are designed to more conveniently measure the isothermal capacitance transients than their isotime counterparts, the latter requiring data reconstruction from the former. In this case, one can project just the isothermal transients to the E_a domain without isotime transients. Figure 4 shows that the nine virtual $\Delta C(E_{a,t})$ transients, produced by projecting the isothermal transients $\Delta C(t, T_{fix})$ in Fig. 1 to the E_a domain via Eq. (8) using the same $\ln(\nu_0'') = 27.7\ \mathrm{s}^{-1}$, overlap with each other with good agreement. Therefore, one can conduct t-E_a projection to project isothermal transients taken at various temperatures to the E_a domain and require all the $\Delta C(E_{a,t})$ transients to agree with each other, thus obtaining a best fit value of ν_0. Again, E_a can be taken directly from the peak position of $dC(E_{a,t})/dE_{a,t}$.

Alternative transient projections are possible by exploiting the E_a-ν_0 symmetry in Eq. (1). Similar to T-E_a and t-E_a projections in Eqs. (7) and (8), we define the T-ν_0 projection,

$$\nu_{0,T} = \exp(E_a''/k_B T)/t_{fix}, \tag{9}$$

and the t-ν_0 projection

$$\nu_{0,t} = \exp(E_a''/k_B T_{fix})/t, \tag{10}$$

where E_a'' is a free tuning parameter. E_a'' adjusts the curvature of virtual transients in the ν_0 domain $\Delta C(\nu_{0,T})$ and $\Delta C(\nu_{0,t})$, which are projected from the experimental isotime $\Delta C(t_{fix}, T)$ and isothermal $\Delta C(t, T_{fix})$ transients, respectively. Matching the virtual transient of $\Delta C(\nu_{0,T})$ to $\Delta C(\nu_{0,t})$ determines the best fit value of E_a''.

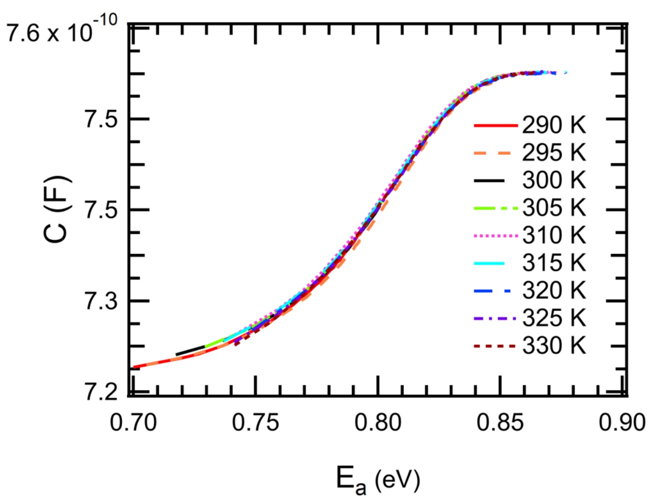

FIG. 4. Isothermal transients taken at all nine different temperatures are projected onto the E_a domain [Eq. (8) with $\ln(\nu_0'') = 27.7\ \mathrm{s}^{-1}$] to produce matching virtual transients $C(E_{a,t})$.

Figure 5 shows the isothermal and isotime transients projected onto the ν_0 domain [by Eqs. (10) and (9), respectively] to produce virtual transients that are in good agreements with each other when the best fit projection parameter of $E_a'' = 810\ \mathrm{meV}$ is used. In case only one kind (isotime or isothermal) of experimental transients is available, one of the corresponding projections [Eqs. (9) or (10)] can be used to project multiple transients of the available kind to ν_0 domain and extract E_a when all projected transients agree to each other. The nine virtual $\Delta C(\nu_{0,t})$ transients, produced by projecting the isothermal transients $\Delta C(t, T_{fix})$ to the ν_0 domain via Eq. (10) using the same $E_a'' = 810\ \mathrm{meV}$, are seen to overlap with each other in Fig. 5. Similarly, $\ln(\nu_0) = 27.7\ \mathrm{s}^{-1}$ is extracted directly from the (negative) peak position of $dC(\nu_{0,t})/d\nu_{0,t}$.

The underlying assumption of the conventional Arrhenius plot method, i.e., fitting the Arrhenius plot by a line to yield a single value of E_a and ν_0, is for both parameters to be invariant[30] over the entire experimental T-t domain. In contrast, the matching of projected transients can be implemented over a small range near T_{fix} and t_{fix}, i.e., by matching the *curvatures* at (T_{fix}, t_{fix}), rendering extractions of E_a and ν_0 that are *local* to (T_{fix}, t_{fix}) and allowed to vary with temperature. The mathematical reason for this advantage is that extracting E_a and ν_0 via matching the curvatures of two mutually orthogonal transients in the T-t plane more efficiently uses the physical information contained in $C(T, t)$ surface than the conventional Arrhenius plot procedure. Although the temperature-dependence of E_a is not prominent in this work because of the limited temperature range, such an effect has been frequently observed (e.g., in III-V[21] and I-II-VI[29] semiconductors) and is indeed expected in wide-bandgap semiconductors such as Ga_2O_3 and GaN[22] due to the carrier capture barrier and the temperature-dependent energetics of the defect and band edges.

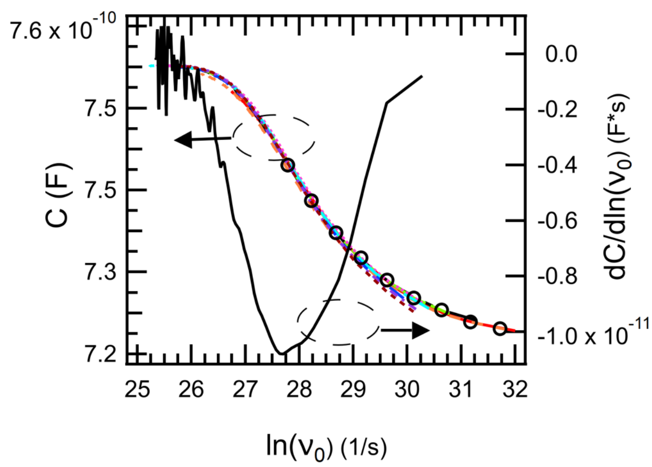

FIG. 5. Isothermal transients (lines) taken at all nine different temperatures are projected onto the ν_0 domain [Eq. (10) with $E_a'' = 810\ \mathrm{meV}$] to produce matching virtual transients $C(\nu_{0,t})$. Also shown is the virtual transient $C(\nu_{0,T})$ (symbols) projected from the isotime transient (taken at $t_{fix} = 2.1\ \mathrm{s}$) onto the ν_0 domain [Eq. (9) with $E_a'' = 810\ \mathrm{meV}$] that matches $C(\nu_{0,t})$. ν_0 is extracted directly from the peak position of $d\Delta C(\nu_0)/d\nu_0$ (right axis).

IV. CONCLUSIONS

In summary, we develop the matched Arrhenius-equation projection technique for extraction of E_a and ν_0 of defects from raw capacitance transients. Below is a typical procedure of the measurement and analysis.

(1) Measurement: record isothermal capacitance transients in the time domain and/or isotime capacitance transients in the temperature domain.
(2) Projection of experimental transients to suitable virtual domains using either E_a' or ν_0' as a free-tuning parameter.
   (a) If both isothermal and isotime transients are available, project the transients between the T and t domains using Eqs. (4) and (6) or project both transients to E_a and ν_0 domains using Eqs. (7)–(10).
   (b) If only one kind of transient, either isothermal or isotime, is available, project the available kind of transient to either the E_a or the ν_0 domain using one of the equations (7)–(10).
(3) Adjust the free-tuning parameter of either E_a' or ν_0' to achieve a matching between a projected virtual transient to a corresponding experimental transient, or between two projected virtual transients. This extracts one of the two parameters of E_a and ν_0. Then, calculate the other of the two from Eq. (1).

We investigated the activation energy E_a and pre-exponential factor ν_0 of a defect 0.8 eV below the conduction band edge in the Ga_2O_3 substrate material without using the Arrhenius plot and using only raw capacitance transient signals. The matched Arrhenius-equation projection technique bypasses certain requirements of DLTS (i.e., rate-window treatment, the peak identification in spectra, the Arrhenius plot construction, and line fitting) and is able to solve E_a and ν_0 local to a temperature point, hence, their temperature dependence. The combination of a general-purpose capacitance instrument and atmospheric sample operation on a hot plate near room temperature is a desirable simplification compared to a commercial DLTS apparatus integrated with a vacuum-based cryogenic system.

ACKNOWLEDGMENTS

The authors acknowledge support from Air-Force Office Science and Research, United States, through Award Nos. FA2386-21-1-4071 and FA2386-22-1-4006.

AUTHOR DECLARATIONS

Conflict of Interest

The authors have no conflicts to disclose.

Author Contributions

Jian V. Li: Conceptualization (lead); Formal analysis (lead); Funding acquisition (equal); Investigation (equal); Methodology (lead); Software (lead); Writing – original draft (lead). **Adam T. Neal:** Investigation (equal); Writing – review & editing (equal). **Shin Mou:** Investigation (equal); Writing – review & editing (equal). **Man Hoi Wong:** Funding acquisition (equal); Investigation (equal); Visualization (equal); Writing – review & editing (equal).

DATA AVAILABILITY

The data that support the findings of this study are available from the corresponding author upon reasonable request.

REFERENCES

[1]A. J. Green *et al.*, APL Mater. **10**, 029201 (2022).
[2]M. Higashiwaki and S. Fujita, *Gallium Oxide: Materials Properties, Crystal Growth, and Devices* (Springer Nature, Switzerland, 2020).
[3]S. Pearton, F. Ren, and M. Mastro, *Gallium Oxide: Technology, Devices and Applications* (Elsevier, Amsterdam, Netherlands, 2019).
[4]M. A. Mastro, A. Kuramata, J. Calkins, J. Kim, F. Ren, and S. J. Pearton, ECS J. Solid State Sci. Technol. **6**, P356 (2017).
[5]S. J. Pearton, F. Ren, M. Tadjer, and J. Kim, J. Appl. Phys. **124**, 220901 (2018).
[6]M. Higashiwaki, K. Sasaki, H. Murakami, Y. Kumagai, A. Koukitu, A. Kuramata, T. Masui, and S. Yamakoshi, Semicond. Sci. Technol. **31**, 034001 (2016).
[7]Y. Zhang and J. S. Speck, Semicond. Sci. Technol. **35**, 125018 (2020).
[8]N. Moser *et al.*, IEEE Electron Device Lett. **38**, 775 (2017).
[9]S. Krishnamoorthy, Z. Xia, S. Bajaj, M. Brenner, and S. Rajan, Appl. Phys. Express **10**, 051102 (2017).
[10]Z. Hu, K. Nomoto, W. Li, N. Tanen, K. Sasaki, A. Kuramata, T. Nakamura, D. Jena, and H. G. Xing, IEEE Electron Device Lett. **39**, 869 (2018).
[11]B.-Y. Liu and J. V. Li, J. Vac. Sci. Technol. B **39**, 012206 (2021).
[12]M. D. McCluskey, J. Appl. Phys. **127**, 101101 (2020).
[13]K. Irmscher, Z. Galazka, M. Pietsch, R. Uecker, and R. Fornari, J. Appl. Phys. **110**, 063720 (2011).
[14]Z. Zhang, E. Farzana, A. R. Arehart, and S. A. Ringel, Appl. Phys. Lett. **108**, 052105 (2016).
[15]A. Y. Polyakov, N. B. Smirnov, I. V. Shchemerov, D. Gogova, S. A. Tarelkin, and S. J. Pearton, J. Appl. Phys. **123**, 115702 (2018).
[16]Y.-Y. Lin, A. T. Neal, S. Mou, and J. V. Li, J. Vac. Sci. Technol. B **37**, 041204 (2019).
[17]A. T. Neal *et al.*, Appl. Phys. Lett. **113**, 062101 (2018).
[18]P. Blood and J. W. Orton, *The Electrical Characterization of Semiconductors: Majority Carriers and Electron States* (Academic, London, 1992).
[19]J. V. Li and G. Ferrari, *Capacitance Spectroscopy of Semiconductors* (Pan Stanford Publishing, Singapore, 2018).
[20]D. V. Lang, J. Appl. Phys. **45**, 3023 (1974).
[21]J. A. Van Vechten and C. D. Thurmond, Phys. Rev. B **14**, 3539 (1976).
[22]D. Wickramaratne, C. E. Dreyer, B. Monserrat, J.-X. Shen, J. L. Lyons, A. Alkauskas, and C. G. Van de Walle, Appl. Phys. Lett. **113**, 192106 (2018).
[23]D. S. Day, M. Y. Tsai, B. G. Streetman, and D. V. Lang, J. Appl. Phys. **50**, 5093 (1979).
[24]G. L. Miller, J. V. Ramirez, and D. A. H. Robinson, J. Appl. Phys. **46**, 2638 (1975).
[25]A. Kuramata, K. Koshi, W. Watanabe, Y. Yamaoka, T. Masui, and S. Yamakoshi, Japan. J. Appl. Phys. **55**, 1202A2 (2016).
[26]A. T. Neal, S. Mou, R. Lopez, J. V. Li, D. B. Thomson, K. D. Chabak, and G. H. Jessen, Sci. Rep. **7**, 13218 (2017).
[27]S.-S. Huang, R. Lopez, S. Paul, A. T. Neal, S. Mou, M.-P. Houng, and J. V. Li, Jpn. J. Appl. Phys. **57**, 091101 (2018).
[28]S. Agarwal, Y. N. Mohapatra, and V. A. Singh, J. Appl. Phys. **77**, 3155 (1995).
[29]J. V. Li, S. W. Johnston, Y. Yan, and D. H. Levi, Rev. Sci. Instrum. **81**, 033910 (2010).
[30]S. Arrhenius, Z. Physik. Chem. **4U**, 226 (1889).